Available online at www.sciencedirect.com
SCIENCE DIRECT®
Journal of Hydrology 291 (2004) 67–90
Journal of Hydrology
www.elsevier.com/locate/jhydrol

Hydromechanical modeling of a large moving rock slope inferred from slope levelling coupled to spring long-term hydrochemical monitoring: example of the La Clapière landslide (Southern Alps, France)

F. Cappa[a,*], Y. Guglielmi[a], V.M. Soukatchoff[b], J. Mudry[c], C. Bertrand[c], A. Charmoille[c]

[a]*UMR 6526 Géosciences Azur CNRS, UNSA, Mecatec Unit, 250 rue Albert Einstein, Les Lucioles I, Sophia Antipolis Valbonne 06560, France*
[b]*LAEGO, Ecole National Supérieure des Mines de Nancy, Parc de Saurupt, 54042 Nancy Cedex, France*
[c]*EA 2642, Géosciences Université de Franche, Comté, 25030 Besançon, France*

Received 10 December 2002; revised 8 December 2003; accepted 12 December 2003

Abstract

Taking the example of the La Clapière landslide, the influence of water infiltration on large moving rock mass stability is investigated. Based on the analysis of geological, hydrogeological, hydrogeochemistry and landslide velocity measurements, a hydromechanical conceptual model is proposed. Then, a two-dimensional numerical modeling with the Universal Distinct Element Code (UDEC) was carried out to determine the influence of the location and the amount of water infiltration on the hydromechanical behaviour of La Clapière slope.

Geological and hydrogeological analyses indicate a perched water-saturated zone connected by large conducting-flow fractures to a basal aquifer. The comparisons of spring water chemistry data and meteorological data from the slope area show a large variability of groundwater transits in the slope through time (transit durations of 1–21 days) and space. Water infiltration transient signals correspond to accelerations of the slope downward motion. Infiltration rates are comprised between 0.4 and 0.8 l s^{-1}. The most pronounced hydromechanical response of the slope instability is due to snowmelting in the stable area located between elevations 1800 and 2500 m above the unstable slope.

The hydromechanical modeling performed with the UDEC code concerns firstly a model of a slope without any unstable zone, and, secondly, a model including a failure surface in order to simulate the current instability. Numerical computations are done in order to localize the area through which water infiltration is the most destabilizing. The most destabilizing area is the one that has the largest influence on the spatial distribution of strain fields. It corresponds to water infiltration located in the middle part of the slope and characterized by weak flow rates of 0.75 l s^{-1}.

This approach can easily be applied to the monitoring of other unstable rocky slopes. As it gives relevant information about the spatial and temporal effects of meteoric infiltration, it can be applied to improve remedial protocols.

Keywords: Large moving rock mass; Groundwater chemistry; Coupled hydromechanical modeling; Universal Distinct Element Code

* Corresponding author. Tel.: +33-4-92-94-26-71; fax: +33-4-92-94-26-10.
E-mail address: frederic.cappa@geoazur.unice.fr (F. Cappa).

0022-1694/$ - see front matter © 2004 Elsevier B.V. All rights reserved.
doi:10.1016/j.jhydrol.2003.12.013

1. Introduction

In the case of large unstable mountainous slopes, it has been clearly shown that the main driving force of instability is gravity and that the major triggering factor is groundwater located in interstices and fractures of rocks (Noverraz et al., 1998). More particularly, groundwater generates a hydromechanical deformation along fractures that can lead to a generalized destabilization of large rock masses (Guglielmi, 1999). However, the understanding of groundwater mechanical effects on landslides and their environment is rendered more complex because of the large heterogeneity of the rock masses and because of the difficulty to apply classic hydrogeological investigation methods in a moving medium. For these reasons, we developed an indirect approach based on chemical groundwater measurements coupled with a two-dimensional hydromechanical modeling with the Universal Distinct Element Code (UDEC) numerical program. This approach has been applied to the case of the La Clapière landslide (Southern Alps, France).

2. Fluid measurements and landslide hydromechanical modeling—case studies and methodology

Pore pressure variations constitute one of the main factors that affect the instability of large moving rock masses (LMRM). LMRM correspond to rock volume mobilization exceeding 1 million m^3 (Noverraz et al., 1998). Unfortunately, there is a lack in LMRM hydrological knowledge probably because it is very difficult to measure and to simulate infiltration (DIPCN/IDNDR, 1999).

Direct field measurements of water pressure are difficult because of:

- the heterogeneity of the rock masses. Indeed, drainage is concentrated in a small number of fractures (1% in the case of the Stripa site, Black et al., 1991; Olsson et al., 1998),
- the huge LMRM volumes; in France, the La Clapière landslide is estimated at about 60 million m^3 (INTERREG1, 1996),
- the movements whose velocities can reach several centimeters per day (about 30–100 mm/day at La Clapière, Follacci, 1987) can damage the measuring devices and can destroy boreholes.

For these reasons, water infiltration monitoring devices is classically deduced from measurements of rain and snow falls on the studied sites. The effects of water pressures are thus indirectly obtained from a correlation between rainfall events and landslide velocity variations (Follacci, 1999).

Indirect methods based on the study of natural hydrogeochemistry of water–rock interactions (Compagnon et al., 1997; Guglielmi et al., 2000) and on artificial tracing experiments (Bonnard et al., 1987) were developed in order to locate water flow paths through the rock mass and to estimate pore pressures at the scale of the LMRM. Tested on French and Swiss landslides, these methods confirm that it is possible to define water infiltration areas, to determine groundwater flow paths, and to estimate water transit and renewal times (Guglielmi et al., 2002).

Introducing pore pressures in the numerical hydromechanical modeling of LMRM allows to check the various hypotheses made on kinematics and on different factors driving the failure of the slope (Barla and Chiriotti, 1995). This implies calculations with codes that take into account hydromechanical laws for discontinuities and where iterations of the model never converge because of the generated instability (Vengeon, 1998). The first problem is to model drainage in a stable fractured medium where it is necessary to simplify the fracture network and the hydraulic laws (Bour, 1996). Such models can run valid three-dimensional calculations in the case of a few numbers of fractures that concentrate all the flow (Vinkler, 1999). Then, if hydromechanical laws are added to mechanical models, additional simplifications are required. For example, in order to run a calculation with a set of fractures, it is necessary to simplify the geometry of a single fracture to a single parameter that is the mean aperture (Fénart, 2002). As a consequence, even in the case of two-dimensional calculations of stable masses, the results are different from field measurements (Kadiri, 1999). For these reasons, LMRM modeling can only provide a parametric analysis and not a predictive analysis (Vengeon et al., 1996). Nevertheless, based on hydromechanical modeling of the Campo Vallemagia LMRM (estimated volume to about 800 million m^3)

in Switzerland, Bonzanigo et al. (2001) could determine the mechanisms of deformation and the possible effects of drainage on the stability of the LMRM. Their numerical model shows that under dry conditions, the slope is relatively stable, whereas after introducing of pore pressures, downslope displacements and velocities increase. Downward displacements are subsequently cancelled once a drainage adit is simulated under the disturbed rock mass.

We develop a hydromechanical model by integrating geological, precipitation, velocity and spring chemistry data from La Clapière landslide. Then, we show that using the chemical monitoring of spring waters is a reliable routine monitoring method of a LMRM. We present a detailed analysis of the infiltration transient signals and their effects on landslide stability that are inferred from comparison between a long term monitoring of groundwater hydrogeochemistry and the landslide accelerations. Lastly, we run a numerical two-dimensional hydromechanical calculation taking into account infiltration yield variations at different locations on the slope profile. We use the UDEC code (Cundall, 1980) to study the coupled hydromechanical effects of changing the infiltration yields and locations on the strain field of the slope.

3. Towards a conceptual hydrogeological model of landslides in crystalline basement areas located in Alpine valleys: example of the La Clapière case study

We first summarize results from previous studies on the La Clapière site which allowed us to build a conceptual hydrogeological model. We then discuss how this model can be representative of groundwater flow in unstable slopes of Alpine valleys located in crystalline basement areas. Previous studies consist of geological and hydrogeological mapping of the area (at the landslide scale and at the valley scale) and in determining groundwater flow paths through the slope by natural chemical and isotopic tracing.

3.1. Hydrogeological and geomorphological investigations

The La Clapière landslide is located on the left bank of the NW–SE oriented Tinée valley, near the Saint-Etienne-de-Tinée village (southern Alps, France; Figs. 1 and 2). It is bordered to its northwestern side by the Tenibres river and to its southeastern side by the Rabuons river, flowing from lakes situated at 2500 m elevations and flowing into the Tinée river. The three valleys define a N010°E trending prismatic geometry that allows a tri-dimensionnal view of the unstable area. The Tinée valley elevation is 1100 m and the two tributaries create a 300 m high notch of the slope. The prism culminates at elevation 2200 m. Elevations of surrounding crests and peaks reach 3000 m. The base of the La Clapière landslide is located at the Tinée valley elevation and is 1 km wide. The landslide currently overlaps the Quaternary alluvial deposits of the Tinée river (Fig. 1(1)). The top of the landslide is a 120 m high scarp that extends over a width of 800 m at elevation 1600 m. The geometry of the basal slip surface is poorly known. Based on cross-sectional geometry, the depth of the failure surface may not exceed 100–200 m (Figs. 1(1) and 2). It follows that the estimated moving volume is about 60 million m^3. The landslide itself is divided into three main compartments limited by pre-existing faults (Figs. 1(1) and 2):

- Compartment 1: the main landslide which corresponds to the central volume bounded by the main failure surface. The downward motions of this rocky mass range between 45 and 90 mm yr^{-1} depending on the measuring points. Displacement vectors show slight changes in orientations that mainly follow N010°E and N115°E orientations which correspond to the two main penetrative fracture directions of the slope (Section 3.2).
- Compartment 2: the upper northeastern compartment corresponds to a 5 million m^3 volume which has completely lost its cohesion and which behaves like a block landslide sliding along its own failure surface which is less deeper than that of the main landslide. It overlaps the main landslide. The downward motions of this compartment range between 100 and 380 mm yr^{-1}.
- Compartment 3: the upper northwestern compartment is bounded to the south by a 150 m high scarp that corresponds to the upper part of the main landslide failure surface and to the north by a 50 m high scarp that marks the current boundary of the La Clapière landslide. This compartment behaves

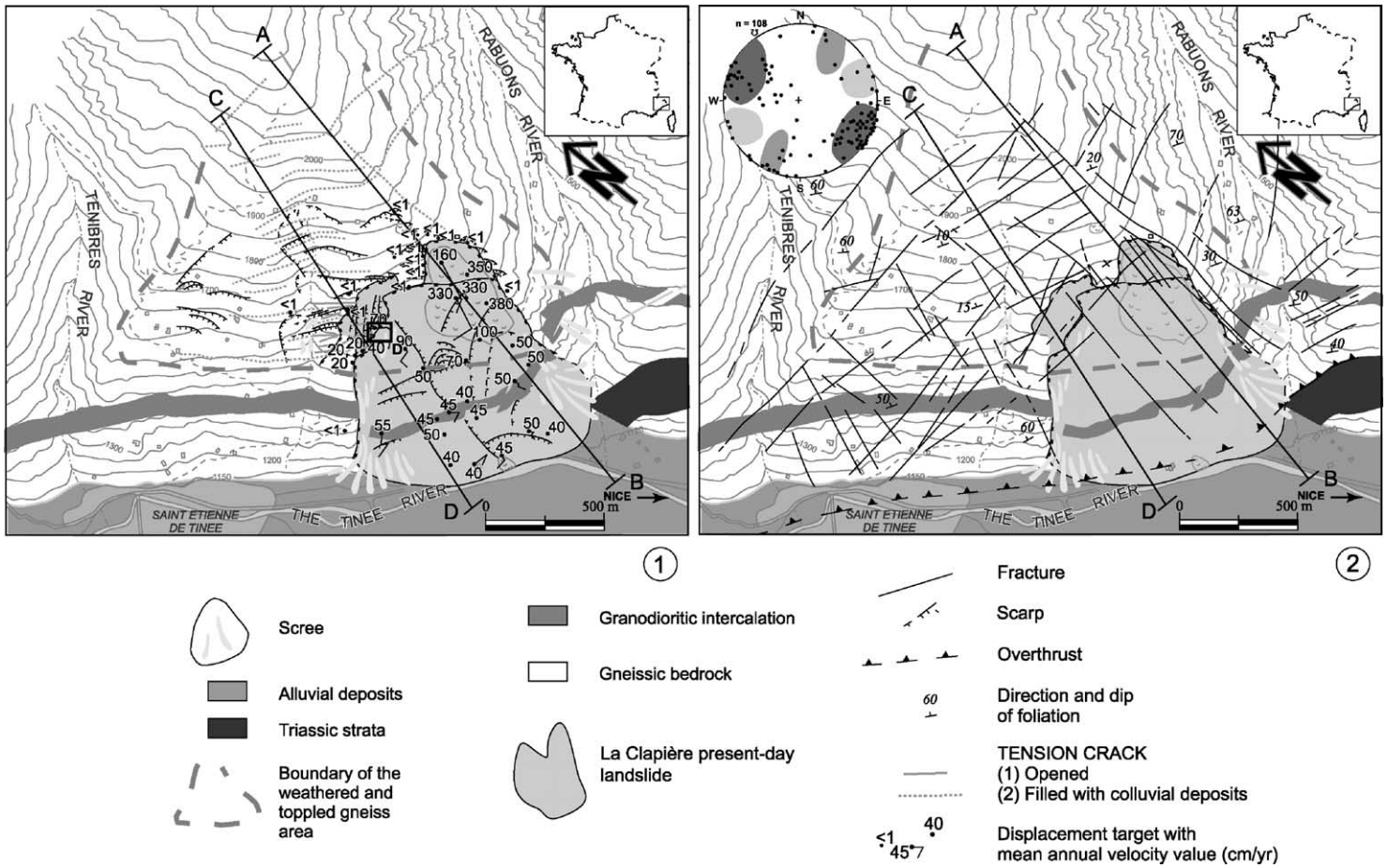

Fig. 1. (1) Geomorphological context of La Clapière landslide; (2) geological context of La Clapière slope.

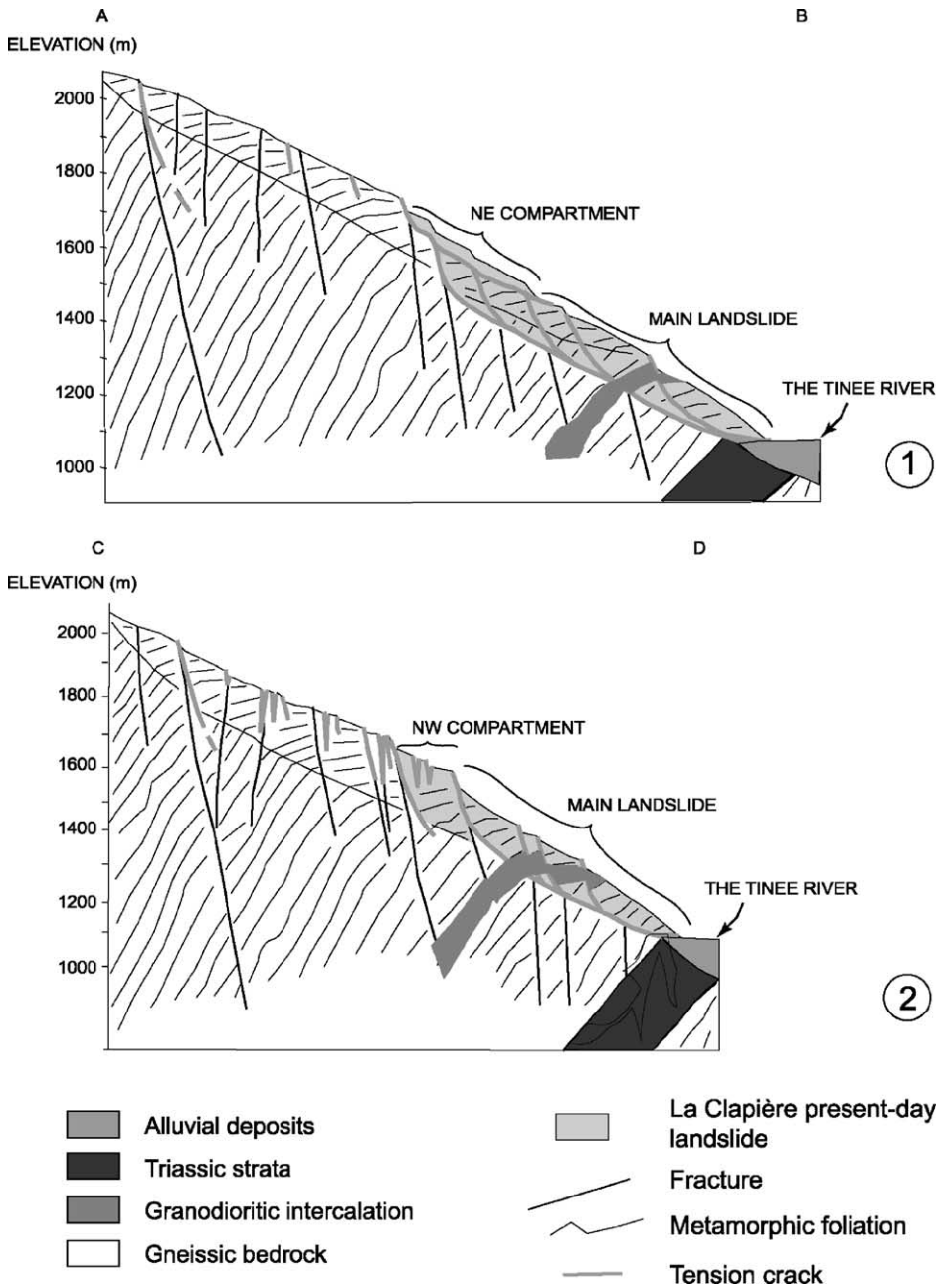

Fig. 2. Geological cross-sections of La Clapière landslide.

like a fractured rock mass with active tension cracks. Measured motions range between 20 and 70 mm yr^{-1}. It is not certain that this compartment should be included in a failure surface at the present time.

The present-day La Clapière landslide is nested in a larger unstable slope which has been active (Fig. 1(1)). This unstable slope is characterized by extensional deformation structures like large tension cracks and several meters high downhill scarps of

the upper part of the slope between 1700 and 2100 m. These landforms involve displacements along penetrative preexisting tectonic joints consistent with gravitational movements. These movements were dated. The Cosmic Ray Exposure (CRE) dating show that these movements occurred during three main pulses: 11,000, 7000 and 3000 years ago (Bigot-Cormier et al., 2003). Tension cracks correspond to a meter-scale horizontal opening of the superficial part of the tectonic joints that induce a 10–20 m deep trench. Many trenches are filled with superficial deposits. Scarps correspond to shear displacements with a vertical throw ranging from 1 and 50 m.

The La Clapière unstable slope is situated at the northwestern edge of the Argentera-Mercantour External Crystalline Massif. This basement unit consists of metamorphic rocks having recorded a polyphased tectonic and metamorphic evolution during the Variscan and Alpine orogeneses (Faure--Muret, 1947; Bogdanoff and Ploquin, 1980; Fig. 1(2)). The slope is composed of two-mica gneisses characterized by alternating or anastomosing thin micaceous layers and quartz-feldspar layers. A meta-granodiorite layer is exposed half-way between the bottom and the top of the landslide (Fig. 2). Whereas the regional metamorphic foliation in the western part of the Argentera-Mercantour strikes N130°E and dips 60° or steeper towards the NE, the foliation in and around the La Clapière slope is horizontal or dips gently (less than 20°) either to the NE or to the SW (Fig. 2; Fabbri and Cappa, 2001; Gunzburger and Laumonier, 2002). The metamorphic foliation in the La Clapière zone appears undulated and microfolded. At the top of the slope, between elevations 1700 and 2200 m elevation, metamorphic rocks are weathered on a thickness ranging from 50 to 200 m. In the middle and at the foot of the slope, the gneisses are fractured. Three sets of faults can be distinguished, trending N010°E–N030°E, N080°E–N090°E and N110°E–N140°E with a dip angles close to 90° (Fig. 1(2)). These sub-vertical faults recorded early-stage strike-slip motions and late-stage reverse or normal motions (Ivaldi et al., 1991). A comparison of the gravitational instability map (Fig. 1) with the geological map (Fig. 2) shows that the brittle fault system has driven the development of the current gravitational instability to a large extent. To the southeast of the Rabuons river, some 0.5 km upstream of its confluence with the Tinée river, gneisses overthrust Triassic deposits, which here occur as a tight overturned syncline with an inner core of gypsum and dolomitic breccia (*cargneules*) enclosed by sandstone layers. (Faure-Muret, 1947; Ivaldi et al., 1991). In the vicinity of the La Clapière unstable slope, the thrust plane between the gneisses and the underlying Triassic strata strikes N140°E and dips northeastwards of about 30°. This overthrust possibly extends northwestwards under the foot of the landslide and under the Tinée alluvial deposits. Quaternary scree and fluvial and glacial deposits, predominantly composed of blocks derived from the metamorphic basement with minor sedimentary rock derived fragments embedded in an argillaceous matrix, locally cover the gneisses, especially upstream of the Rabuons river.

From the hydrogeology point of view, the landslide can be regarded like a discontinuous fractured reservoir. Water flows into fractures whose openings depend on the depth and on the structure of the slope. Rock matrix (gneisses) can be considered as impervious. Fluvio-glacial deposits correspond to superficial continuous reservoirs. The landslide can be taken as a highly permeable fractured reservoir because the displacements induce the formation of large pores inside opened fractures, breccias and blocks (Fig. 3). The landslide is drained at its foot by a group of perennial springs (springs 14, 15, 16, 20 on Fig. 3) with a total discharge comprised between 0.25 and 0.35 $l\,s^{-1}$. The springs rise at the bottom of a major N010°E trending major fault zone that cuts the middle part of the main landslide. A perennial spring (spring 1, Fig. 3) rises at the foot of the northeastern compartment at elevation 1550 m, and has a discharge comprised between 0.1 and 0.3 $l\,s^{-1}$. After long precipitation periods, some temporary springs rise at the same elevation (springs 2, 9, 10, 13 on Fig. 3). All these temporary springs (springs 9, 10 and 13) rise along faults or at the bottom of major tension cracks filled with colluvial deposits (spring 2 is located at the bottom of a long N010°E tension crack). All the streams that originate from the perched springs (springs located in the upper part of the landslide) are interrupted a few hundred meters downstream. This means that all the waters reinfiltrate in the main landslide.

Outside the landslide, the slope can be divided into a decompression toppled zone and a low

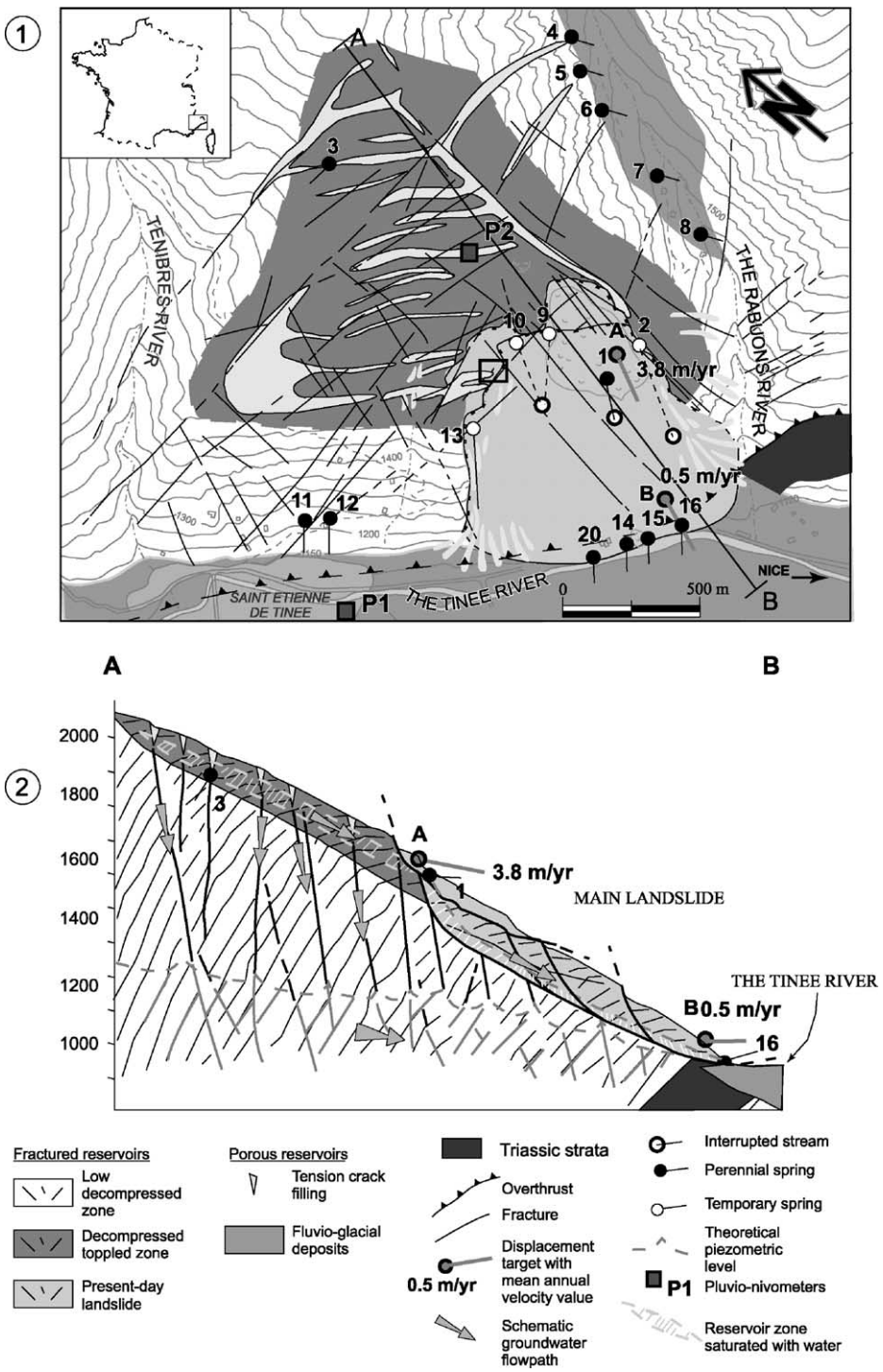

Fig. 3. (1) Hydrogeological context of La Clapière landslide; (2) schematic hydrogeologic cross-section of the slope.

uncompressed zone in depth. The decompression toppled zone extends between 1600 and 2000 m. It is a highly fractured area where tension cracks create highly permeable linear drains. Many of the cracks are filled with colluvial deposits, which constitute small reservoirs with an interstitial porosity. These tiny reservoirs are interconnected via the tension crack network. It is possible to look in detail at colluvium filled cracks because some of them are cut by the present-day La Clapière main scarp (for location see black rectangle near the spring 10 on Fig. 3(1)). Typically, the filling has a 4–20 m wide triangular geometry (Fig. 4). It consists in blocks of various sizes and which arrangement defines rough bedding. The bedding is warped, showing that sedimentation occurred while gravitational movement was active. The deepest part of the filling often consists of very thin deposits of a buried soil that collapsed when the tensile crack was formed. Blocks and sands that can be found in the upper part of the deposits come from the fractured edges of the crack. The crack extends inside the slope because it is the superficial reactivation of a tectonic fault. Depending on the places, the colluvial fillings can be completely dry or can be drained by a perennial spring (springs 3 and 4 on Fig. 3(1)). In the first case, water infiltrating in the colluvial deposits is drained deeper in the slope through the underlying tectonic fault. In the second case, water is trapped in the filling because the basal buried soil is locally impervious. The interconnection of the fillings creates a perched perennial saturated zone that could explain the presence of springs rising in the upper part of the slope between 1650 and 1550 m. The low uncompressed part of the slope is outcropping on the Rabuons, the Tenibres and the Tinée river banks below the elevation 1400 m (Fig. 3(1)). This zone is fractured by major tectonic joints and can be considered as a relatively low-permeability fissured reservoir. There is continuity between the joints and the tensile cracks mapped in the uncompressed toppled zone. Many springs rise at the bottom of the joints in the Tinée valley slope (springs 11 and 12 with a discharge ranging between 0.1 and 0.4 $l\,s^{-1}$) and in the Rabuons valley (springs 4, 5, and 6 with a discharge ranging between 0.1 and 0.6 $l\,s^{-1}$). Some groundwater outlets possibly rise directly in depth into the alluvial deposits but cannot be observed.

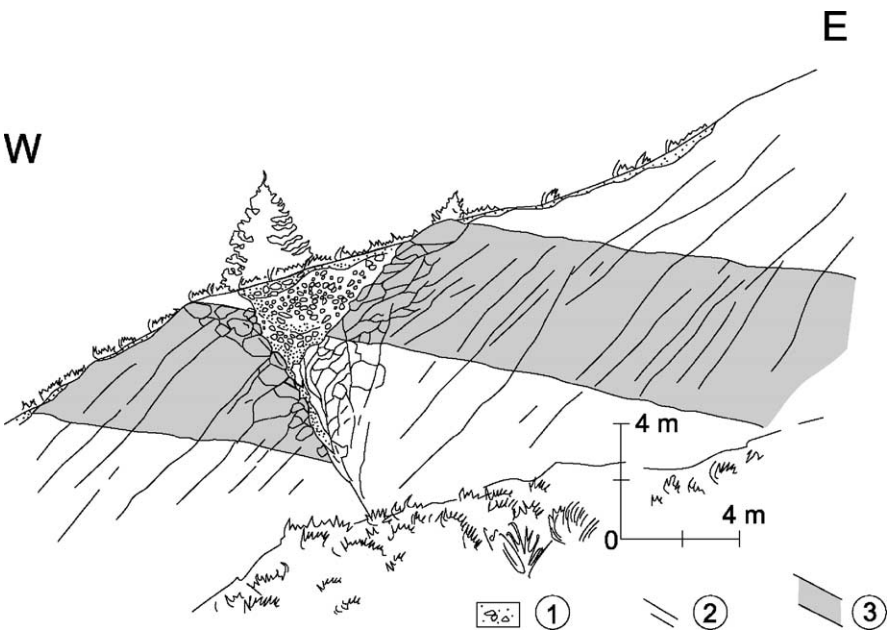

Fig. 4. Lateral view of a tensile crack; (1) colluvial deposits; (2) fractures; (3) gneissic facies with a 10° E dipping foliation.

3.2. Conceptual hydrogeological model: description and discussion

All these hydrogeological and geomorphological observations allowed us to propose the following model. There are at least two main water-saturated zones in the slope: firstly, a perched saturated zone which is contained in the crack filling colluvial deposits and adjacent weathered gneisses of the uncompressed toppled zone, and secondly, a basal saturated zone which is present in the low uncompressed zone deep in the slope. Groundwater drainage can follow three main types of flowpaths (Fig. 3(2)):

- direct outlets, springs located between 1550 and 1650 m (springs 1, 2, 3, 4, 5, 6, 9, 10, 13, on Fig. 3(1)) drain the perched aquifer; springs 11 and 12 drain the basal aquifer; springs 14, 15, 16 and 20 drain the landslide.
- infiltration into the landslide of groundwater coming from the perched or the basal aquifer.
- infiltration from the perched aquifer down to the basal aquifer by the penetrative joints which are in continuity with the superficial cracks.

Such a model highlights the main hydrogeological characteristics of an unstable slope developed in crystalline basement rocks. The hydrogeology of the slope is better described by several disconnected saturated zones rather than by a single one. This is the general case of mountainous slopes in crystalline basement areas where hydraulic conductivity decreases with depth because of the decompression phenomena. The conductivity of the decompression zone that can be 600 m thick varies between 10^{-4} and 10^{-8} m s^{-1}. The conductivity of the non-decompressed zone is comprised between 10^{-9} and 10^{-11} m s^{-1} (Maréchal, 1998). The conductivity contrast between the two zones induces two types of groundwater flows, a major one parallel to the boundary and a minor one perpendicular to the boundary. These were observed into several alpine galleries where the more important discharges occur in the first hundreds of meters in the decompression zone (Leca et al., 1993). When the decompression includes toppling or landsliding, the hydraulic connection between fractures of the two zones (decompression and non-decompression zones) is weathered. In that case, some aquifers can remain perched in the decompression zone (François and Massonnat, 1981). In the La Clapière case, we show that such a disconnection can be explained by the clogging of the upper part of fractures when this part is reactivated as tensile cracks and filled with colluviums. A part of the infiltration waters can transit into the landslide mass from the perched aquifer and from the basal aquifers. The $\delta^{18}O$ content of the springs waters indicates that, depending on the season, the mean elevation of the recharge area of the springs is the same and is comprised between 1570 ± 150 and 1780 ± 150 m (Compagnon et al., 1997; Guglielmi et al., 2000). This value includes an area larger than the landslide itself (because the maximum elevation of the upper part of the landslide is 1600 m) and which corresponds to all the outcropping part of the uncompressed zone. We conclude that waters infiltrated in that zone flow parallel to the slope down to the landslide and perpendicular to the slope down to the basal aquifer. The same results were obtained by Maréchal (1998) who used the $\delta^{18}O$ method to show that major water discharges in Alpine gallery came from infiltration in a toppled zone quite far from the gallery. Finally, in the Mercantour massif, the average hydraulic conductivity of decompressed rock was estimated to 2.7×10^{-6} m s^{-1} from the interpretation of discharge variations with time in the gallery of Valabres, located about 10 km southeast of the La Clapière area (Bordet, 1961). In the same gallery, it was observed that discharge increased significantly with precipitation events like snowmelting on the nearby mountains and that discharge was around zero during dry periods. Heterogeneity of the drainage was also evidenced with a few productive fractures draining a mean annual yield of 200 l s^{-1}.

4. Measurements of groundwater infiltration effects on the La Clapière slope movement

Firstly, we characterize precipitation on the whole slope. Secondly, we compare the precipitation signal with groundwater chemistry at the springs. Thirdly, we compare chemistry variations with landslide velocity measurements at the two selected topometric points. Velocity variations of point A are compared to chemical variations of spring 5 which are

representative of water drainage in the upper part of the slope (indirectly pore pressure variations in the perched aquifer). We intend to show how useful groundwater chemistry can be to estimate the influence of precipitation inflows on the landslide movement.

4.1. Measurement device

In order to characterize the infiltration and its effects on the La Clapière slope movement we set a monitoring device that relies upon the measurement of three data types:

- Precipitation measurements are done with rain and snow gauges at the foot of the slope (1100 m elevation), at the middle of the slope (1800 m elevation) and at the top of the slope (2500 m elevation). This discrete monitoring enables a quantification of the daily amount of water (snowmelt or rain) precipitated at the three measurement points. In order to better characterize precipitation events between these points, and because of the huge dimensions of the slope, we added a qualitative spatial monitoring of the snow cover by taking photography of the slope from a point located on the opposite side of the valley. This monitoring allows to follow the retreat of the snow cover boundary with elevation during snowmelting.
- Spring water chemistry has been monitored since December 1995 at three springs located at 1650 m elevations (Fig. 3, spring 5), 1200 m (Fig. 3, spring 11) and 1100 m (Fig. 3, spring 15). Spring 5 collects waters from the perched superficial zone at 1650 m. Springs 11 and 15 collect waters from the deep basal saturated zone, respectively, in the stable zone (1185 m elevation) and at the landslide foot (1100 m elevation). With such monitoring, we intend to characterize groundwater outlets from the slope, relying on the hypothesis that groundwater chemistry depends on transfer duration inside the media, on slope petrography and on subsurface soil characteristics. The spring waters are sampled once a month to once every 2 days, depending on the flow period. We analyzed major ions of the waters. In this paper, we will examine the variation in SO_4^{2-} and NO_3^- contents.
- Landslide velocities are permanently monitored by the French Ministry of Equipment. Two points among the 45 topometric permanent measured points were selected as representative of the mass movement: one at the top of the landslide, and the other one at the foot of the moving zone. The first point (Fig. 3, point A with the mean annual velocity of 3.8 m y^{-1}) shows velocity variations representative of the displacement of the upper south-eastern part of the moving zone (between elevations 1500 and 1720 m). The second point (Fig. 3, point B located above spring 15 with the mean annual velocity of 0.5 m y^{-1}) shows velocity variations representative of the displacement of the basal and median parts of the moving zone (between elevations 1100 and 1500 m).

4.2. Results

Since the device is regularly destroyed by the landslide movement and because of the high-mountain climatic conditions, the chemical sampling rate is irregular. For this reason, we concentrated on the sampling period that extends from 12/9/98 to 31/12/00 (Fig. 5), during which sample recovery was excellent.

4.2.1. Characterization of precipitation events on the slope

Due to the measuring protocol, we can differentiate three types of precipitation: rainfall everywhere in the slope, snowmelt between 1100 and 2200 m, and snowmelt between 1800 and 2500 m The overlap is due to the fact that the snow gauge located at elevation 1800 m is used to evaluate the amounts of two snowmelting zones (Fig. 5). Infiltrations on the La Clapière slope mainly consist of rainfall from October to December and of snowmelting from March to July. Average autumn rainfall rates range around 500 mm per year (annual average value calculated for the period 1982–2000), and extend on short durations from 30 to 60 days (INTERREG1, 1996; Follacci, 1999). The average spring snowmelt amount is 810 mm. Nevertheless, snowmelting can be very different, depending on the elevation range. Between the valley (1100 m high) and 2200 m, the snow storage is low and it can be neglected at the slope scale. From 1800 m to the top of the slope (2500 m),

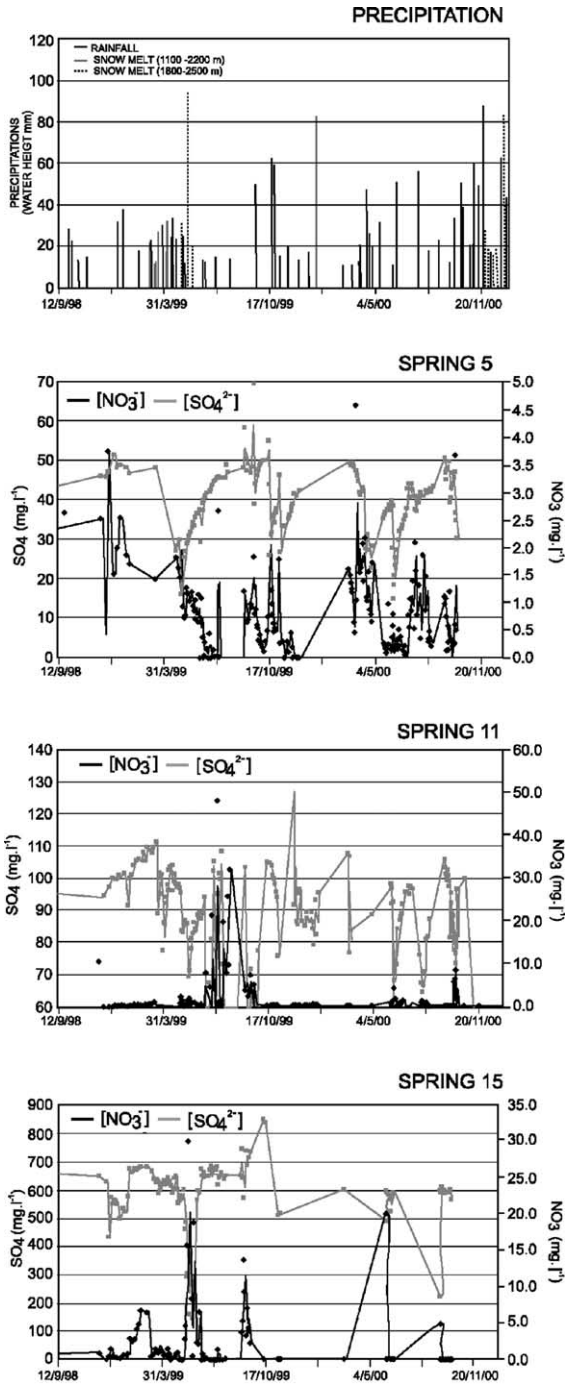

Fig. 5. Comparison of precipitation events on la Clapière slope with SO_4^{2-} and NO_3^- contents variations at the springs 5, 11 and 15 that drain different slope aquifers (location of springs 5, 11 and 15 on Figs. 1(1) and (2)) for the 1999–2000 hydrologic period.

there is no snowmelting in winter. Snow is accumulated until the beginning of the spring period. A quick and major snowmelting follows, for example 985 mm in 29 days in 1986. We can conclude that precipitation on the slope can be schematically characterized by a predominant rainfall between 1100 and 1800 m and a predominant snowmelt between 1800 and 2600 m. The 1998–1999 precipitation amounts range around the average annual value. The 1999–2000 period was very dry; precipitation amounts are 50% lower than the average value. In 2000, precipitation was characterized by a very small amount of snowmelting (less than 130 mm of equivalent water).

4.2.2. Correlation of spring water chemical variations with precipitation events

The chemical signal shows transient events characterized by SO_4^{2-} concentration decreases that occurred after precipitation events (Fig. 5). When there is no precipitation (for example August 1999), the content in SO_4^{2-} remains high and the variation range is low. SO_4^{2-} transient variations are the opposite of NO_3^- transient variations. After a precipitation event, there is an increase of NO_3^- contents of 1–30 mg l^{-1} depending on the event and on the spring. At the same time, there is a decrease in SO_4^{2-} content from 40 to 100 mg l^{-1} (Fig. 5). It is commonly admitted that water is enriched in NO_3^- when it infiltrates through the superficial soil area (Mudry et al., 1994). As a matter of fact, this means that a NO_3^- peak in spring waters corresponds to the transit of the infiltrated meteoric waters to the reservoir outlet. Previous studies (Guglielmi et al., 2000; Charmoille, 2001) showed that there is no SO_4^{2-} in the precipitation and that the water–rock interactions all along the transit inside the reservoir explain SO_4^{2-} groundwater enrichment. We found that an enrichment of SO_4^{2-} up to 160 mg l^{-1} can be explained by the dissolution of pyrite within the slope gneisses. Over 160 mg l^{-1} (this is the case of spring 15 sulfate content) and up to 800 mg l^{-1} in sulfate content result from the dissolution of pyrite within the slope gneisses and from the dissolution of Triassic gypsum likely to be trapped under the thrust fault located at the foot of the slope. Thermodynamic calculations show that the more sulfate-rich the waters are, the longer they stayed inside the slope. The fact that there is a significant decrease in SO_4^{2-} means that,

during precipitation periods, there are rapid infiltration fluxes through the reservoir corresponding to shallow waters, chemically far from equilibrium with the reservoir rock chemistry. Transient signals are then interpreted as dilution inflows, linked to low concentration precipitation water inflow, which mix with pre-event groundwaters from the saturated zone that is chemically near equilibrum with the rock matrix primary minerals (Fig. 6A). Taking this result into consideration, we can model infiltration fluxes, based on a double permeability fractured reservoir, where there is a complex connection of a few very conductive fractures with a large number of poorly conductive fractures (Drogue, 1992; Bonzanigo et al., 2001; Guglielmi et al., 2000; Maréchal and Etcheverry, 2002). During dry periods, the water contained in the poorly conductive fractures is drained through very conductive fractures to the spring (Fig. 6B).

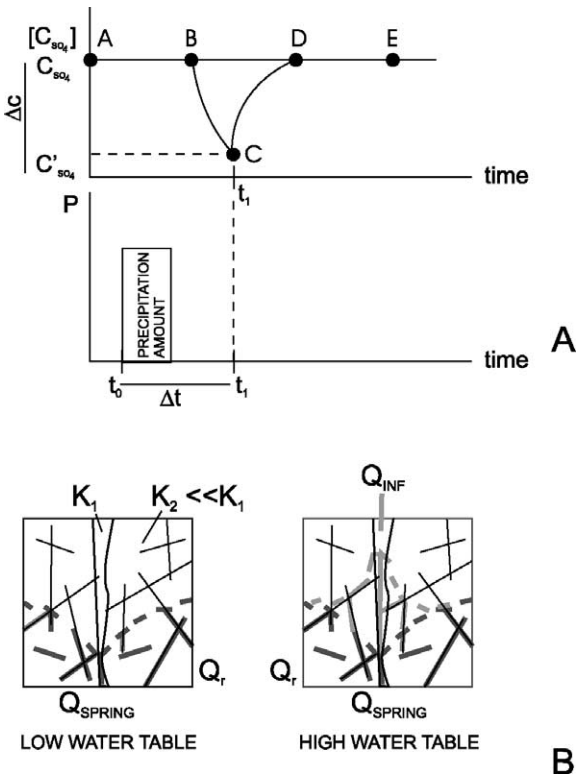

Fig. 6. Model of infiltration inside La Clapière slope; (A) scheme of chemical transient; (B) functioning of double permeability fractured rock mass.

The hydraulic gradient is from poorly conductive zones towards very conductive fractures. The chemical signal is mainly controlled by an average residence time corresponding to the one in the low conductive fractures. During infiltration periods, there is a quick transit of surface water through the very conductive fractures (between 1 and 21 days in the case of La Clapière slope) and a very delayed transit of surface waters through the poorly conductive zones. Rapid transit waters that do not reach chemical equilibrium with the reservoir rock are waters characterized by low ion concentrations (their concentration is close to that of the precipitation water one). They mix with concentrated water originating from the poorly conductive zones of the reservoir. Such a model is in agreement with other similar models developed in crystalline basement rock environments in the Alps (Maréchal, 1998; Bonzanigo, 1999).

4.2.3. Quantitative estimation of infiltration yield in the slope

With the model described above, we can infer the amounts of infiltration yields based on the equations of conservation of fluxes neglecting the volume variations inside the reservoir This method is commonly used for hydrograph separation of river runoff and karstic spring flood events (Mudry, 1990; Hjalmar and Olav, 1997). It is assumed that solute concentration variations depend on the composition of the different discharge sources. In our case, we can apply a two component mixing model (Pinder and Jones, 1969) as follows:

$$Q_S = Q_R + Q_I \tag{1}$$

$$Q_S C_S = Q_R C_R + Q_I C_I \tag{2}$$

where Q_S is the total discharge at the spring, C is concentration of sulfate (which is the element taken as the applicable tracer) and the subscripts R and I refer to the main aquifer water component that supplies the spring to the point of complete drying-up, and the infiltration water component, respectively. From Eqs. (1) and (2), we can express the spring sulfate concentration C_S as follows:

$$C_S = \frac{(Q_R C_R + Q_I C_I)}{(Q_R + Q_I)} \tag{3}$$

When there is no infiltration on the slope, Eq. (3) becomes:

$$C'_S = \frac{Q_R C_R}{Q_R} \quad (4)$$

Taking into consideration Eqs. (3) and (4), ΔC (which corresponds to the tracer content variation during the flood event) can be expressed:

$$\Delta C = C_S - C'_S = \frac{(Q_R C_R + Q_I C_I)}{(Q_R + Q_I)} - \frac{Q_R C_R}{Q_R}$$

$$= \frac{Q_I}{(Q_R + Q_I)}(C_R - C_I) \quad (5)$$

When $\Delta C = 0$, it means that $Q_I = 0$ after Eq. (5). If Q_I increases, ΔC also increases. This means that there is an increase of the dilution peak value on the curves C_S versus time. Eq. (5) can be simplified if C_I is approximately taken equal to 0. With such an assumption, a simple relationship between spring sulfate water content variations and infiltration yields (6) can be obtained:

$$\Delta C = \frac{Q_I}{(Q_R + Q_I)} C_R \quad (6)$$

Q_I was calculated for various ΔC measured at springs 5 and 15. In the calculation, Q_R and C_R values were fixed at 0.5 ± 0.01 and 50 ± 10 mg l^{-1} for spring 5; 0.25 ± 0.01 and 710 ± 30 mg l^{-1} for spring 15, and 0.25 ± 0.01 and 105 ± 10 mg l^{-1} for spring 11. Comparison between ΔC and calculated Q_I to cumulated precipitation amounts (Fig. 7A) shows

HYDROLOGIC CYCLE 1998 - 2000	SPRING 5 (ALTITUDE 1645 m)	SPRING 11 (ALTITUDE 1185 m)	SPRING 15 (ALTITUDE 1100 m)
SNOWMELT [1100 - 2200 m]	[1 - 4 days]	[3 - 10 days]	[4 - 8 days]
SNOWMELT [1800 - 2500 m]	[5 - 8 days]	[10 - 15 days]	[10 - 21 days]
RAINFALL	[1 - 4 days]	[2 - 14 days]	[2 - 16 days]

B

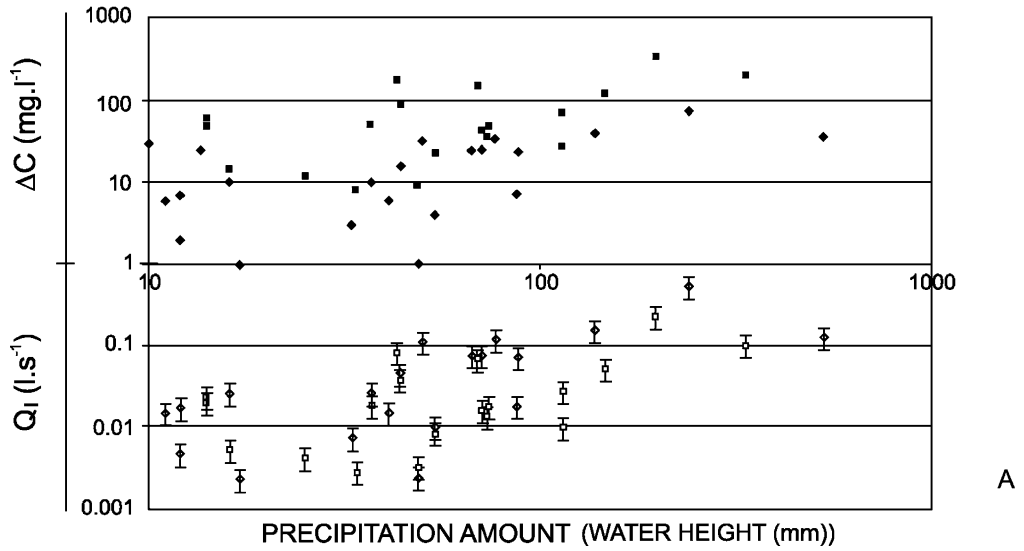

A

Fig. 7. (A) Correlation between Δt and Q_I and precipitation amounts; (B) array of Δt values for various infiltration types and for the three monitored springs.

that there is an important scattering of measurements even with the adopted bi-logarithmic representation that enables to plot on the same graph ΔC of springs 11 and 15. Firstly, the precipitation amount is not the best parameter to describe the infiltration input because it does not take into account evapotranspiration that varies significantly according to the season. Secondly, ΔC determination depends on the C_R value that was considered as constant for the studied period. This is not obvious when we look at the curves and there is no indication that the C_R linearly varies with time. Nevertheless, the diagram shows a tendency to the increase of ΔC with precipitation amounts (this means that sulfate content decreases when infiltration increases). It is interesting to note that the deduced Q_I values range between 0.01 and $1\,l\,s^{-1}$, which can be regarded as relatively low values. The highest Q_I values ranging from 0.08 to $0.8\,l\,s^{-1}$ correspond to infiltration periods induced by snowmelting between 1800 and 2500 m.

4.2.4. Quantitative estimation of the delay of infiltration peak in the slope

In the model we make the hypothesis that the SO_4^{2-} minimum value (point C on Fig. 6A) marks the end of increasing infiltration influx and the beginning of infiltration decline. Then we can measure the time delay Δt between the beginning of the precipitation event (t_0 on Fig. 6A) and the infiltration peak effect in the aquifers (t_1 on Fig. 6A).

We compare Δt measured at the three monitored springs for the three previously defined precipitation types (snowmelt at 1100–2200 and at 1800–2500 m and rainfall, Fig. 7B). There is a strong variability of Δt independently of the infiltration type of the spring. Nevertheless, the short Δt values correspond to rainfall infiltration and snowmelt between 1100 and 2200 m elevations with values comprised between 1 and 16 days and the long Δt values correspond to snowmelt infiltration between 1800 and 2500 m with values ranging between 5 and 21 days. The values Δt measured at spring 5 are twice as small as the values Δt measured at springs 15 and 11 especially for snowmelting between 1800 and 2500 m. This discrepancy can be explained by the fact that spring 5 is located higher up in the slope (elevation 1645 m) than springs 11 and 15 (respectively, 1185 and 1100 m). Spring 5 drains the perched saturated zone where infiltration water transits in 1–8 days. Springs 11 and 15 drain the basal saturated zone where infiltration transit in 2–8 days when precipitation occurs below 2200 m. When infiltration comes from the top of the slope, the values Δt are comprised between 10 and 21 days.

4.2.5. Correlation of infiltration with landslide velocities

We compare velocity variations of the upper and basal part of the landslide (respectively, A and B) with chemical variations of springs 5 and 15 that, respectively, characterize infiltration in the upper perched aquifer and in the basal aquifer (Fig. 8). Landslide velocities are characterized by very slow periods (velocities ranging from 1 to 5 mm day^{-1}) and acceleration periods. Acceleration amplitudes are higher in the upper part than in the basal one; for example the acceleration peak value on the 99/11/25 is 44.3 mm day^{-1} at point A and only 14.9 mm day^{-1} at point B. Acceleration periods are synchronous at the two points. It is obvious that acceleration periods correlate with infiltration periods marked by chemical dilutions at the springs. Accelerations happened for the most important infiltration yields (Q_I) ranging between 0.4 and $0.8\,l\,s^{-1}$ and the longer the infiltration period, the greater the acceleration amplitude. This means that the highest accelerations correspond to precipitation periods occurring between 1800 and 2500 m. The infiltration peak at spring 5 occurred just before the beginning of an acceleration period while the infiltration peak at spring 15 occurred when the acceleration peak value happened. This shows that the coupled hydro-mechanical effect comes from the transit of infiltration waters from the top to the basal part of the slope. More precisely, we can reasonably guess that interstitial pressure elevations in the perched aquifer mainly induce an acceleration of the whole landslide. Then, the phenomenon is controlled by a groundwater vertical transit from the perched aquifer to the basal aquifer.

4.2.6. Conclusion: conceptual model

Given in situ investigations based on a hydro-geochemical analysis of groundwaters linked with landslide velocity measurements, a conceptual hydro-mechanical model of the slope can be established (Fig. 8).

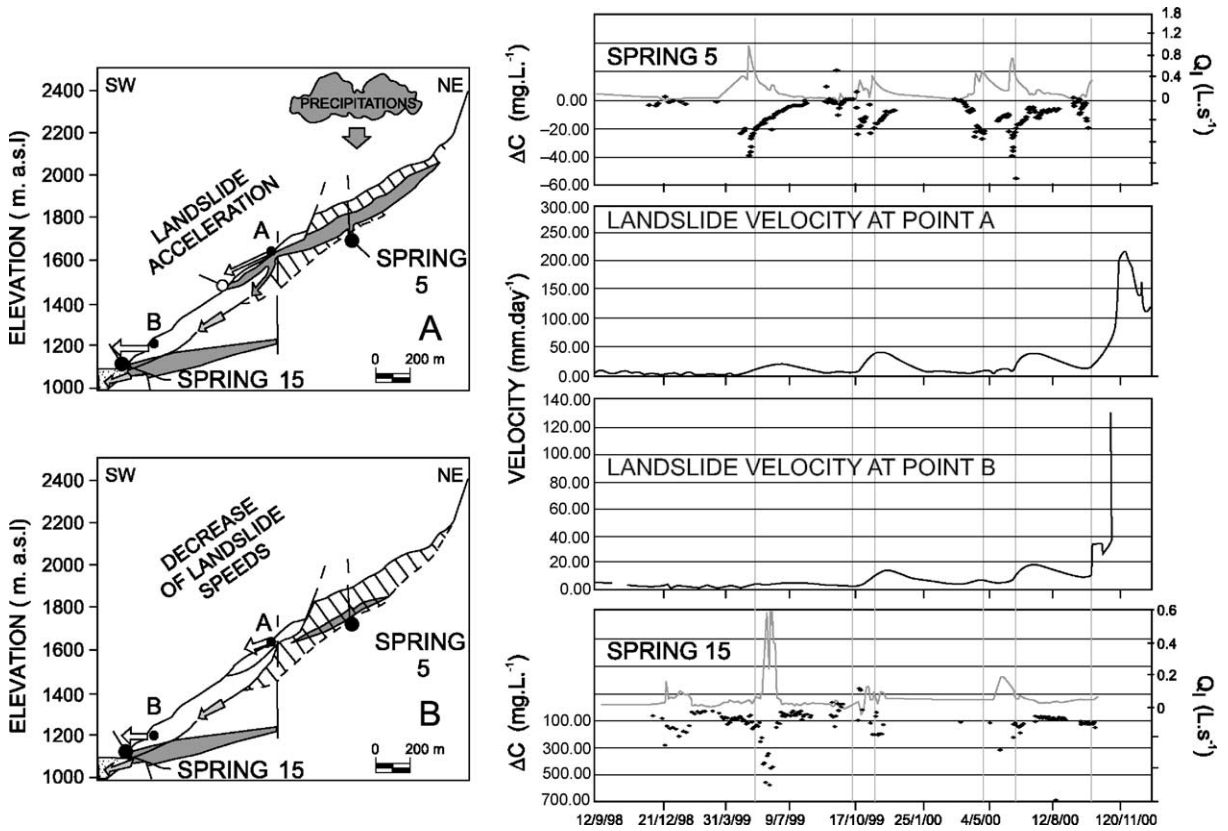

Fig. 8. (A) and (B) Hydromechanical conceptual scheme of La Clapière slope; on the right, comparison between chemical variations of springs 5 and 15 (Q_I and SO_4^{2-} contents) and landslide accelerations at points (A) and (B) for 1999–2000 hydrologic period.

The hydromechanical model boundaries correspond to a large slope with elevations ranging between 1100 and 2500 m in order to take into account the whole recharge area of the landslide. Inside the slope, there is a perched saturated zone between elevations 1600 and 1800 m and a basal saturated zone between 1100 and 1200 m. The whole slope is considered as a doubly permeable aquifer with a small number of highly conductive fractures and a large number of poorly conductive fractures. The main hydromechanical effect originates from snowmelting in the upper part of the slope between 1800 and 2500 m. From this upper recharge area, water infiltrates at the top of the landslide with a transit time through the perched saturated zone that can reach 5–8 days. An infiltration yield ranging from 0.4 to 0.8 l s^{-1} causes a generalized landslide acceleration. Groundwater then transits to the basal saturated zone within a period comprised between 8 and 12 days. Hydraulic transit between the two saturated zones can happen through the landslide or through existing vertical and very conductive fractures. When the infiltration yield peak occurs at the basal spring, it means that the major part of infiltration has outflowed the slope and the landslide velocity begins to decrease.

5. Numerical hydromechanical modeling

5.1. Objectives of numerical tests performed with UDEC code

The aim of the numerical modeling is to make parametric tests of the conceptual model that was deduced from our hydrogeochemical observations and measurements. Calculations were performed in order to test three types of parameters and their effects on

the hydromechanical behaviour of the slope:

- Climatic parameters. Meteorological infiltration scenarios corresponding to various locations and seepage intensities were applied to a two dimensional slope profile.
- Geometrical parameters. We tested the impact of local interstitial pressure elevations inside fractures on the overall stability of the slope. We tested fracture internal geometry and fracture network geometry with the numerical code UDEC. Three different geometries were analysed, a slope with two perpendicular fracture families with different spacing, in order to simulate two different permeability tensors, and a slope with a failure surface located at its base as observed in the field.
- Hydrogeological parameters. We tested the effect of a perched saturated zone inside the slope.

5.2. Universal distinct element code modeling

The UDEC code uses the distinct element method (Cundall, 1980) to model the bi-dimensional effects of stress on fluid flow and to investigate the anisotropy of permeability (Pine and Cundall, 1985; Zhang and Sanderson, 1996). One of the advantages of UDEC arises from its explicit solution of equations of motion based on small time steps. This allows large finite displacements and deformations to be modelled, with the program recognizing new contact geometries that may arise during deformation. In UDEC, the deformation of fractured rock consists in the elastic and/or plastic deformation of blocks of intact rock, and of displacements along and across fractures (Cundall, 1990). A fully coupled mechanical-hydraulic analysis is performed, in which fracture conductivity is dependent on the mechanical displacement of joint walls and on matrix deformation; conversely, fluid pressures affect the mechanical behaviour. The fractured rock mass is modelled as a closely packed system of blocks with elastic properties. The blocks are impervious and bound by fluid-filled fractures. They communicate with their neighbours through the contacts. At these contacts, the fluid flow is calculated using the cubic law (Witherspoon et al., 1980):

$$q = \frac{a^3 g}{12\nu}\left(\frac{\Delta P}{L}\right) \tag{7}$$

where q is the flow rate, ν the dynamic viscosity of the fluid (for $T = 20$ °C, ν is equal to 10^{-3} Pa s, g is the gravity acceleration, a is the hydraulic aperture of the joint (m), ΔP is the pressure differential into the joint domains, L is the contact length (m).

For simplicity, fracture aperture is assigned to a constant value between two nodes of the mesh of the blocks and so a fracture is approximated by two parallel planes. A minimum aperture value (residual aperture) is given. Below it, mechanical closure does not affect the contact permeability. The more numerous the contacts are, the more accurate the calculations will be. The model does not incorporate fracture growth.

5.3. Initial conditions

A two-dimensional hydromechanical analysis is developed considering a vertical cross-section oriented NE–SW that is perpendicular to the topographic surface and to one of the main fracture families (Fig. 9). This cross-section extends from the slope crest (elevation: 2600 m) to the Tinee valley slope base (elevation: 1100 m). In order to minimize boundary effects in the calculation zone, the cross-section profile extends down to sea-level (Fig. 9). The cross-section is constrained by displacement-type boundary conditions: no bottom vertical displacements and no lateral horizontal displacements were allowed. The grid point is composed of triangular mesh elements whose sides are 100 m long in the fractured part of the model situated between elevations 900 and 2600 m, whereas the sides of mesh elements in the bottom part below elevation 900 m are 200 m long.

The mechanical behaviour of the rock matrix is taken as linearly elastic and isotropic. Rock discontinuities are assumed to behave according to an elasto-plastic law with the Mohr–Coulomb failure criterion. The fractures included on the extended crosssection correspond to the main N90 fractures mapped in the site. These fractures are connected to each other by horizontal joints that were added with a 200 m spacing between elevations 900 and 2750 m. In the context of the study area, these joints approximate foliation planes.

Mechanical characteristics of matrix and fractures were determined from literature data (Barla and Chiriotti, 1995; Gunzburger, 2001). The bulk modulus for gneissic formation is $K = 5.3 \times 10^{10}$ Pa, the shear modulus is $G = 2.5 \times 10^{10}$ Pa and the mass density (d) is

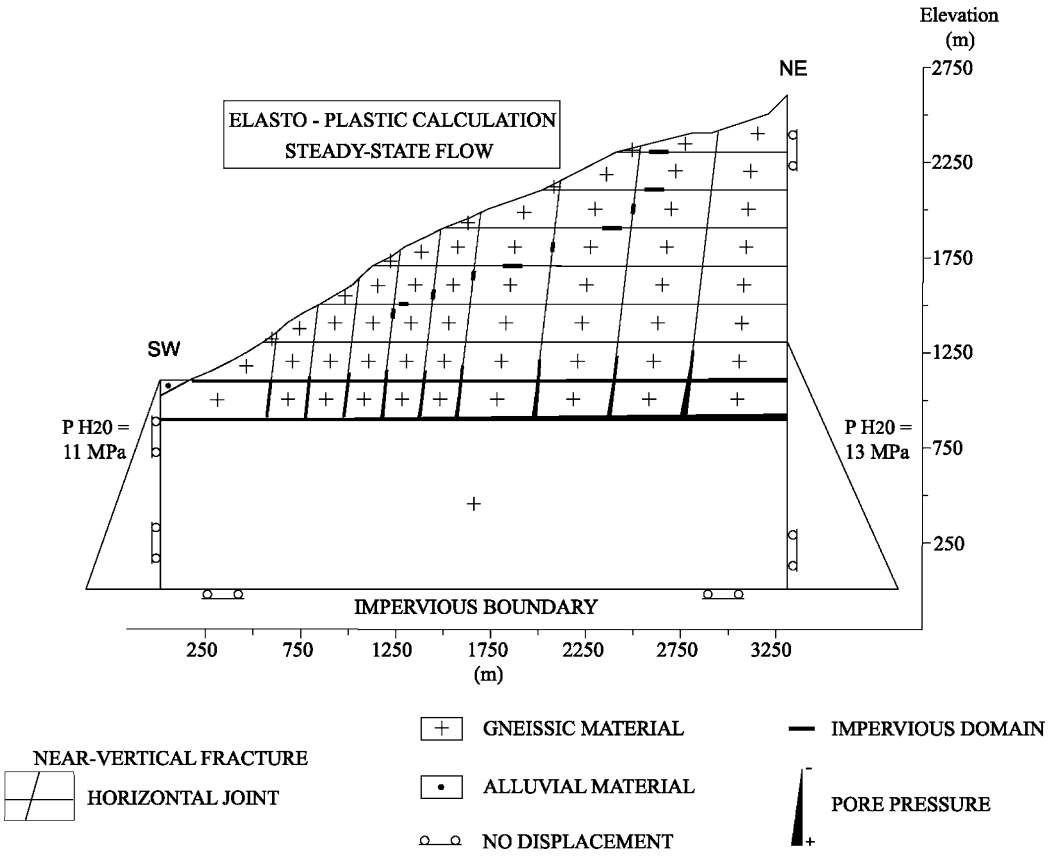

Fig. 9. UDEC numerical modeling initial conditions.

2200 kg m^{-3}. For alluvial deposits, we assigned $K = 2.9 \times 10^9$ Pa, $G = 1.3 \times 10^9$ Pa and $d = 1500$ kg m^{-3}. Values of normal stiffness $Jk_n = 1.8 \times 10^{10}$ Pa m^{-1}, shear stiffness $Jk_s = 1.8 \times 10^9$ Pa m^{-1} and friction angle $\phi = 30°$ are similar for the vertical and horizontal discontinuities. Alluvium-gneiss contact is assumed to be without shear stiffness, purely frictional with $Jk_n = 1.0 \times 10^9$ Pa m^{-1}, $Jk_s = 1.0 \times 10^{-13}$ Pa m^{-1} and $\phi = 30°$. No rock mass cohesion ($c = 0$) is applied to all fractures.

The hydraulic properties assigned to the discontinuity network are the factor permeability of the joint aperture for zero normal stress $a_{zero} = 1.0 \times 10^{-3}$ m and the residual aperture (a_{res}) was fixed at 1.0×10^{-4} m. In order to simulate a perched saturated water level, a zero permeability was assigned to the fracture domains corresponding to an impervious hydrogeological zone boundary in the slope. Initial groundwater conditions (that correspond to the basal saturated aquifer) were simulated by imposing boundary conditions with an hydraulic gradient from the right side (elevation 1300 m) to the left side at the natural saturation level of the Tinee river (elevation 1100 m). The flow in the joints was set to be compressible.

Gravity acceleration was applied. In situ stress was not considered in our model because of the lack of knowledge on the present-day stress state. We performed a static hydro-mechanical calculation with steady-state flow.

5.4. Modeling protocol

This slope is first consolidated by gravity until stress and displacements are numerically stabilized. After this initial calculation without any water, groundwater conditions were simulated by imposing boundary conditions with a hydraulic gradient from

the right side to the left side ($\Delta p = 2$ MPa). Thirdly, we started the 'numerical tests' simulating water injections at various locations and for different injection flow rates. Water injections were achieved by assigning an injection flow rate at a fracture domain. Then, hydromechanical effects are followed by controlling pressure and displacement fields at several points in the cross-section.

Two series of numerical tests are performed: without (TEST 1 series) and with (TEST 2 series) a failure surface inside the slope (Fig. 10). In both cases, the influence of the location and the intensity of precipitation on the internal and surface displacements of the slope are examined:

TEST 1: slope without failure surface

Three different tests are run with various infiltration conditions. A first test series is considered simulating three water injections at a constant flow rate ($q = 1.0\,\mathrm{l\,s^{-1}}$) at three different elevations in the slope: slope foot (1500 m; Test 1.1), middle part of the slope (1900 m; Test 1.2) and slope top (2300 m; Test 1.3). All the injections were performed one by one for each elevation.

The second test series consisted in simulating an infiltration gradient with elevation ($q = 0.5\,\mathrm{l\,s^{-1}}$ at 1500 m (Test 1.4), $q = 0.75\,\mathrm{l\,s^{-1}}$ at 1900 m (Test 1.5), $q = 1.0\,\mathrm{l\,s^{-1}}$ at 2300 m (identical to Test 1.3).

After these three numerical calculation tests, the most unfavourable case from the point of view of the slope displacements is determined considering

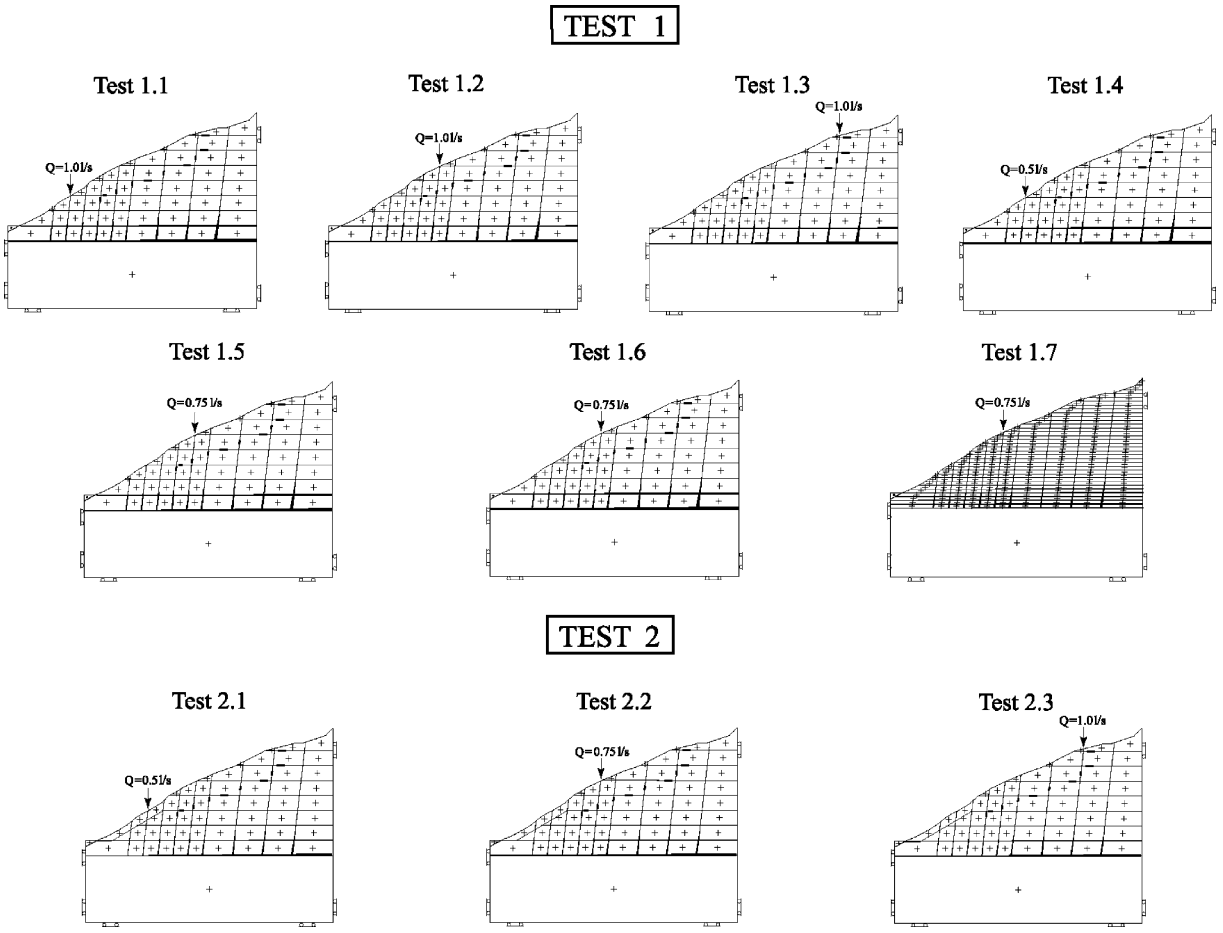

Fig. 10. Numerical test procedure.

the following comparison criterion: the importance of the area in which the displacement values are maximum.

This unfavourable case is compared with two new numerical tests considering the same water injection conditions:

Test 1.6: a model without perched saturated water level assigning the same permeability factor for each fracture domain ($k_f = 83.3\ Pa^{-1}\ s^{-1}$).

Test 1.7: a model with an increasing average permeability of media. For this, we increased fracture density (horizontal joints spacing of 50 m from 900 m elevation).

TEST 2: slope with a failure surface between elevations 1100 and 1500 m.

The same tests as in Test 1 series are performed. We only present the test with an infiltration gradient ($q = 0.5\ l\ s^{-1}$ at 1500 m (Test 2.1), $q = 0.75\ l\ s^{-1}$ at 1900 m (Test 2.2), $q = 1.0\ l\ s^{-1}$ at 2300 m (Test 2.3)) on a slope geometric model integrating a possible failure plane so as to introduce an unstable zone similar to the present-day La Clapière slope. These three injections were performed one by one for each elevation. Mechanical and hydraulic characteristics of the failure plane are similar to those of other discontinuities ($Jk_n = 1.8 \times 10^{10}\ Pa\ m^{-1}$, $Jk_s = 1.8 \times 10^9\ Pa\ m^{-1}$, $\phi = 30°$, $c = 0\ Pa$, $k_f = 83.3\ Pa^{-1}\ s^{-1}$, $a_{zero} = 1.0 \times 10^{-3}$ m and $a_{res} = 1.0\ e^{-4}$ m).

5.5. Results of numerical tests

5.5.1. Results of TEST 1 series

Following the first series of numerical tests (Tests 1.1–1.5), it clearly appears that the unfavourable case from the point of view of spatial distribution of displacement intensities in the cross-section corresponds to a water injection at 1900 m elevation for a flow rate of $0.75\ l\ s^{-1}$ (Test 1.5, Fig. 11). The maximum calculated values of displacement vector are located between the foot of the slope at 1100 m and the middle part of the slope at 1900 m. This strain zone extends from 50 to 400 m inside the slope. Displacements values vary between 0.1 and 1.3 m in that zone. Water pressures are situated in two distinct zones which hydraulically communicate with each other: a basal 500 m thick saturated zone with interstitial pressures ranging between 0 and 5 MPa, and a perched 200 m thick saturated zone with interstitial pressure ranging between 0 and 2 MPa. In the other tests, infiltration takes place too low (Test 1.1) or too high in elevation (Test 1.3), or infiltration yield is too small (Test 1.4) to create a large deformation zone. Test 1.2 results are similar to those of Test 1.5 (infiltration at 1900 m elevation, and infiltration yield of $1.0\ l\ s^{-1}$). In this test, the highest yield induces more important displacements in the infiltration area than for Test 1.5. Such displacements close fractures around this area, and this explains why the infiltration-induced deformations remain located in the middle of the slope.

Without any perched saturated zone (Test 1.6, Fig. 11), pore pressures raise significantly in a 720 m thick saturated zone from 0 to 7.2 MPa. The strain zone is located between 1350 and 1900 m, it extends 600 m deep with more important displacement values than in previous tests (upper to 1.3 m).

Test 1.7 (Fig. 11) also shows that an increase of the slope permeability induces a pore pressure decrease (pressure variation ranging 0–5.5 MPa) and a 200 m thick strain zone located at the foot of the slope between 1100 and 1350 m elevation (Fig.11). Displacement values range from 0.4 to 1.3 m.

5.5.2. Results of Test 2 series

It appears that the most important strain zone is due to a water injection at 1900 m elevation with a flow rate of $0.75\ l\ s^{-1}$ (Test 2.2, Fig. 12). A basal saturated zone and perched saturated zone appear in our model with a strain zone from 400 to 550 m thick located between 1100 and 1650 m elevation. Displacement value variations range from 0.1 to 0.6 m.

Injection test at 1500 m elevation (Test 2.1, Fig. 12) shows a strain zone developing at the slope foot between elevations 1100 and 1500 m. The strain zone extends 200–300 m deep and displacement values range between 0.1 and 0.5 m.

A water injection at high elevation (Test 2.3, Fig. 12) on the slope has no significant hydromechanical effects.

5.6. Conclusion of numerical simulations

The same results are obtained with or without a failure surface materialized at the foot of the slope.

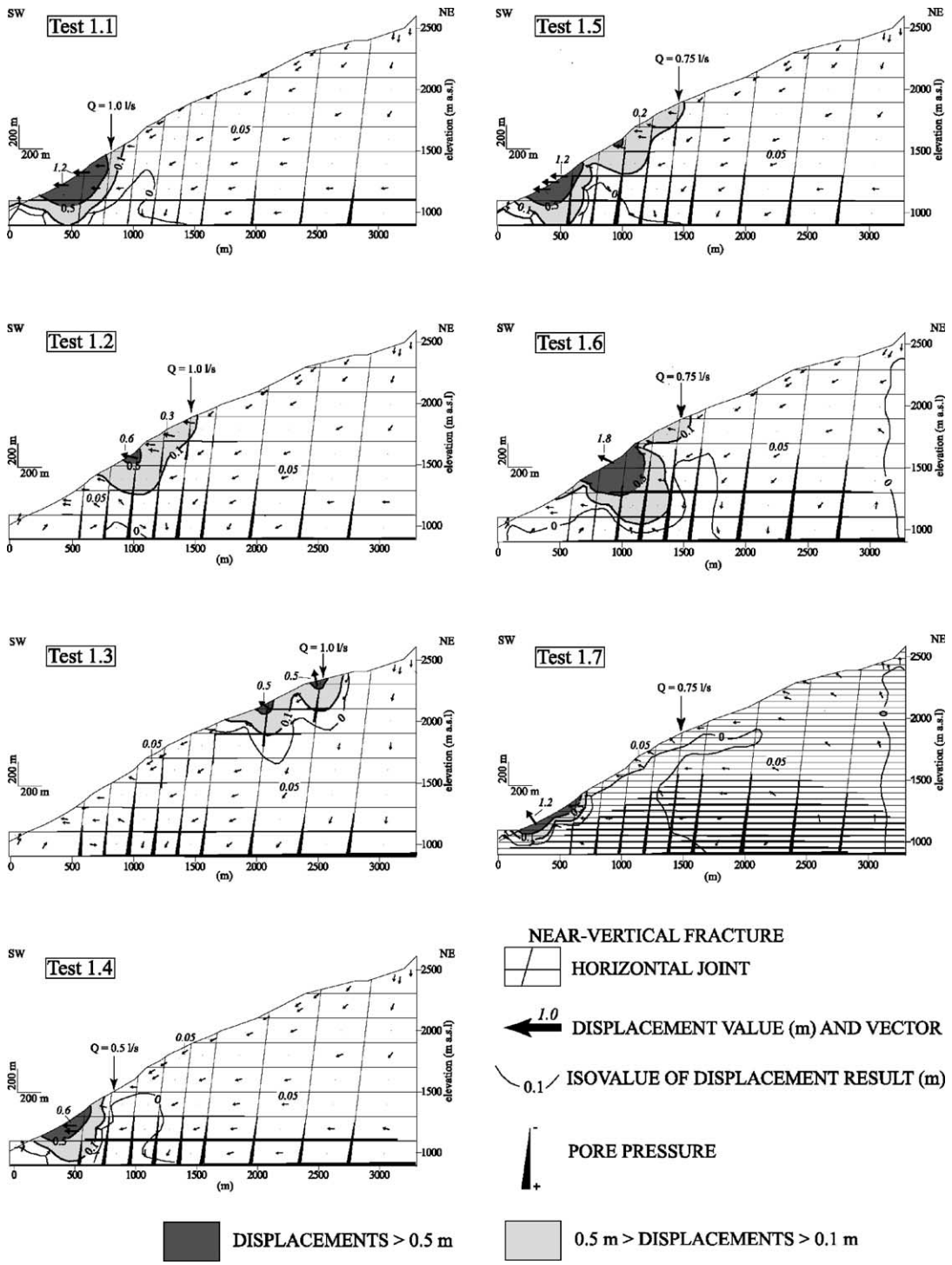

Fig. 11. Results of TEST 1 series.

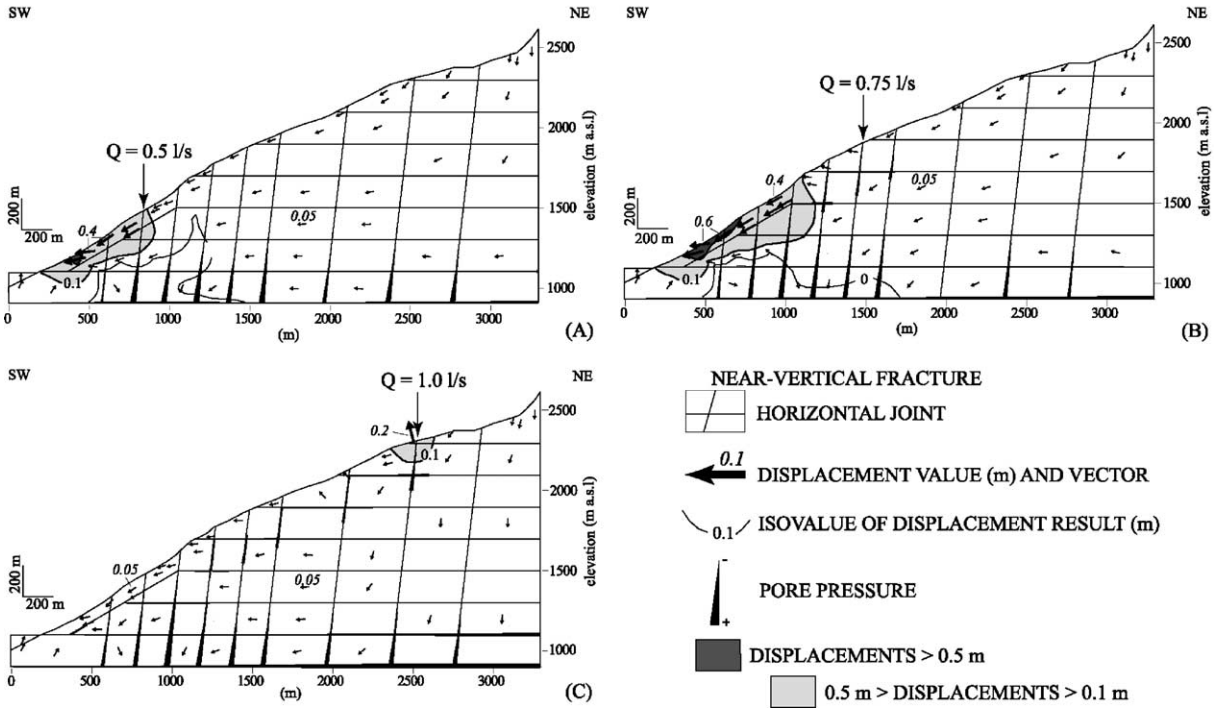

Fig. 12. Results of TEST 2 series.

When there is a failure plane at the base of the slope, displacements are concentrated along this failure surface. In both cases, numerical tests highlight that the most extended strain zone is due to a water injection at 1900 m with a low flow rate of $0.75\,l\,s^{-1}$. We show that perched saturated zone occurrence or increase in permeability of rocky media causes a significant pore pressure decrease and a strain reduction. This means that to have any effect on slope stability, an infiltration flow rate ranging between 0.4 and $0.8\,l\,s^{-1}$ must be concentrated in a few fractures. In such hydraulic conditions, interstitial pressures can reach high values and localized hydromechanical effects can be important.

6. Conclusion

Applied to the La Clapière unstable slope, field and numerical investigations enable us to improve the understanding of the deformation of the whole slope showing that location and intensity of the water infiltration on the cross-section profile played an important role in the slope hydromechanical behaviour. The approach is based on chemical and yield measurements of spring waters on the slope. Such measurements outline transient signals that integrate infiltration transit into the slope. It appears that the transits are quite simple and easy to correlate with landslide velocities and precipitation events. Acquisition of transits can be done with periodic samplings at the springs. Numerical tests that have been added to field measurements interpretation aim at inferring internal hydromechanical couplings, which is difficult to do in the field where the hazards linked to active landsliding is high. One should be aware that such tests remain parametric and only aim at helping to interpret hydromechanical mechanisms at the slope scale.

Nevertheless, the method points out some results that can be extrapolated to other similar LMRMs:

- It is possible to classify precipitation events taking into account their impact on landslide displacements. For example, in the La Clapière case, the most dangerous event corresponds to a quick snowmelting in a well localized range of elevations (1800–2500 m). This result points out the need to follow, with a high accuracy, the spacial variability of precipitation in the case of unstable mountainous slopes.
- Due to the internal complexity of the slope hydrogeology, especially the existing perched aquifer in the decompression toppled zone directly connected to the landslide, the most dangerous infiltration inflow is not necessarily that on the landslide area. In our case, the area between 1800–2500 m is located in the upper stable part of the slope, above the landslide.
- Groundwater flow through the slope can be very fast (1–20 days) even in low permeability rocks such as gneisses. This is due to the double permeability of the fractured media that characterize the slope drainage. It follows that a coupled hydromechanical stability model can be established from a simplified fractured media where only a few major fractures will be analysed and where all the other fractures will be grouped in homogeneous volumes bounded by these major fractures.
- Relatively low infiltration yields between 0.4 and $0.8\,l\,s^{-1}$ can induce significant accelerations of the unstable rock mass. This result fits with experiments on other similar LMRMs (Bonzanigo et al., 2001). As a matter of fact, water flows in a small number of conductive fractures inside which even a small inflow causes important interstitial pressure elevations. In such a context, the existence of different saturated zones perched at different elevations in the slope is a prominent factor that controls pressure variations. We can guess that the more numerous the saturated zones are, the lower the pressures variations will be.

Finally, thanks to the preliminary investigations developed in this paper, a list of a series of realistic scenarios of the hydromechanical behavior of a LMRM could be established. We insist on the fact that the accuracy of such a method relies on long-term data collections of at least 1 year long. The scenarios can lead to curative solutions. For example, in the La Clapière case, it appears important to drain the perched saturated zone which is quite feasible: it would involve two or three relatively short (around 100 m deep) pumping boreholes located in the stable part of the slope.

Acknowledgements

This research program was funded by the French National Program on Natural Hazards (PNRN) during the years 1998–2002. The authors sincerely thank Pr. O. Fabbri for his constructive comments.

References

Barla, G., Chiriotti, E., 1995. Insights into the behaviour of the large deep seated gravitational slope deformation of rosone, in the piemont region (Italy). Felsbau 13, 6.

Bigot-Cormier, F., Braucher, R., Guglielmi, Y., Bourlès, D.L., Dubar, M., Stéphan, J.F., 2003. Chronological constraints of la Clapiere landslide (44°15N, 6°56E, France): geomorphology and cosmonuclide approaches. Geophys. Res. Abstr. 5, 12840.

Black, J., Olsson, J., Gale, J., Holmes, D. 1991. Site characterization and validation—stage 4—preliminary assessment and detail prediction. Stripa project. TR91-08, SKB, Report, Stockholm, Sweden, pp. 1–38.

Bogdanoff, S., Ploquin, A., 1980. Les gneiss et migmatites du massif de l'Argentera (Alpes-Maritimes): apport de deux coupes géochimiques. Bull. Soc. Géol. Fr. 29 (3), 353–358.

Bonnard, C.H., Noverraz, F., Parriaux, A., 1987. Origin of Groundwater Likely to Affect a Large Landslide, Proceedings of the Ninth European Conference on Soil Mechanics and Foundation Engineering, Balkema, pp. 389–392.

Bonzanigo, L., 1999. Lo slittamento di Campo Vallemagia. PhD Thesis, ETH, Zurich, Switzerland, 219 p.

Bonzanigo, L., Eberhardt, E., Loew, S., 2001. Hydromechanical Factors Controlling the Creeping Campo Vallemaggia Landslide, Proceedings: Landslides-Causes, Impacts and Countermeasures, Davos, Switzerland, pp. 13–22.

Bordet, C., 1961. Recherches géologiques sur la partie septentrionale du Massif de Belledone (Alpes françaises). Mém. Soc. Géol. Fr. Paris.

Bour, O., 1996. Transferts de fluides dans les milieux fractures. Effets d'échelle. PhD Thesis. University of Rennes I, 200 p.

Charmoille, A., 2001. Modélisation hydrogéochimique couplée des interactions eau-roche en fonction des écoulements: Application à l'aquifère du versant de La Clapière

(Alpes-Maritimes, France). Master Thesis. University of Franche-Comté, 30 p.

Compagnon, F., Guglielmi, Y., Mudry, J., Follacci, J.P., Ivaldi, J.P., 1997. Approche chimique et isotopique de l'origine des eaux en transit dans un grand glissement de terrain: exemple du glissement de La Clapière (Alpes-Maritimes). C.R. Acad. Sci., Paris 325 (II), 565–570.

Cundall, P.A., 1980. A Generalized Distinct Element Program for Modeling Jointed Rock. Peter Cundall Associates, US Army, European Research office, London Report PCAR-1-80.

Cundall, P.A., 1990. Numerical Modeling of Jointed And Faulted rock, Mechanics of Jointed and Faulted Rock, Belkema, Rotterdam, pp. 11–18.

DIPCN/IDNDR, 1999. International conference on mountain natural hazards—Recommandations. Pôle Grenoblois d'Études et de Recherche pour la Prévention des Risques Naturels, Grenoble, 3 p.

Drogue, C., 1992. Hydrodynamics of karstic aquifers: experimental sites in the Mediterranean karst, southern France. Int. Contrib. Hydrogeol. 13, 133–149.

Fabbri, O., Cappa, F., 2001. Apports de l'analyse structurale à la compréhension de la dégradation du glissement de la Clapière, Massif du Mercantour, Alpes-Maritimes. S. Spé. Soc. Géol. Fr., 13–14.

Faure-Muret, A., 1947. Sur des affleurements de Trias pincés dans les schistes cristallins de la vallée de la Tinée (Alpes-Maritimes). C.R. Acad. Sci., Paris 224, 205–207.

Follacci, J.P., 1987. Les mouvements du versant de la Clapière à Saint-Étienne-de-Tinée (Alpes-Maritimes). Bull. Liaison Labo. Ponts et Chaussées 150/151, 107–109.

Follacci, J.P., 1999. Seize ans de surveillance du glissement de la Clapière (Alpes-Maritimes). Bull. des laboratoires des Ponts et Chaussées 220, 35–51.

François, J.M., Massonnat, G., 1981. Relations entre fracturation et circulations aquifères dans le massif d'Allevard (Alpes France). Rev. Géol. Dyn. Géogr. Phys. 23 (4), 309–318.

Fénart, P., 2002. Caractérisation du comportement hydromécanique des massifs rocheux fissurés. PhD Thesis. University of Montpellier II, 308 p.

Guglielmi, Y., 1999. Apport de la mesure des couplages hydro-mécaniques à la connaissance hydrogéologique des réservoirs fissurés. HDR, University of Franche-Comté, 187 p.

Guglielmi, Y., Bertrand, C., Compagon, F., Follacci, J.P., Mudry, J., 2000. Acquisition of water chemistry in a mobile fissured basement massif: its role in the hydrogeological knowledge of the La Clapiere landslide (Mercantour massif, Southern Alps, France). J. Hydrol. 229, 138–148.

Guglielmi, Y., Vengeon, J.M., Bertrand, C., Mudry, J., Follacci, J.P., Giraud, A., 2002. Hydrogeochemistry: an investigation tool to evaluate infiltration into large moving rock masses (case study of La Clapière and Séchilienne alpine landslides). Bull. Engng Geol. Env. 61 (4), 311–324.

Gunzburger, Y., 2001. Apports de l'analyse de la fracturation et de la modélisation numérique à l'étude du versant instable de la Clapière. Master Thesis. INPL, Nancy, 81 p.

Gunzburger, Y., Laumonier, B., 2002. Origine tectonique du pli supportant le glissement de terrain de la Clapière (NW du massif de l'Argentera-Mercantour, Alpes du Sud, France) d'après l'analyse de la fracturation. C.R. Acad. Sci., Paris 334 (6), 415–422.

Hjalmar, L., Olav, S., 1997. Hydrograph separation using stable isotopes, silica and electrical conductivity: an alpine example. J. Hydrol. 201, 82–101.

INTERREG1, 1996. Risques générés par les grands mouvements de versant, étude comparative de 4 sites des Alpes franco-italiennes. Programme Interreg 1 France-Italie. Regione Piemonte-University J. Fourier, LIRIGM Grenoble, 207 p.

Ivaldi, J.P., Guardia, P., Follacci, J.P., Terramorsi, S., 1991. Plis de couverture en échelon et failles de second ordre associés à un décrochement dextre de socle sur le bord nord-ouest de l'Argentera (Alpes-Maritimes France). C.R. Acad. Sci., Paris 2 (310), 31–36.

Kadiri, I., 1999. Modélisation du comportement mécanique d'un massif calcaire fracturé. Master Thesis. Institut National Polytechnique de Lorraine, Nancy, France, 57 p.

Leca, E., Atwa, M., Rat, M., Humbert, P., 1993. Analyse des écoulements hydrauliques autour des tunnels. In: Reith, (Ed.), Infrastructures souterraines de transports, Balkema, Rotterdam, pp. 55–63.

Maréchal, J.C., 1998. Les circulations d'eau dans les massifs cristallins alpins et leurs relations avec les ouvrages souterrains. Thesis 1769. EPF, Lausanne, 298 p.

Maréchal, J.C., Etcheverry, D., 2003. The use of 3H and 18O tracers to characterize water inflows in Alpine tunnels. Appl. Geo Chem., 18(3), 339–351.

Mudry, J., 1990. Les courbes de flux chimique-débit et le fonctionnement des aquifères karstiques. J. Hydrol. 120, 283–294.

Mudry, J., Lastennet, R., Puig, J.M., Blavoux, B., 1994. Use of natural tracing to understand how an aquifer works. Intake area, recharge fluxes, transit-an example from the Ventoux-Vaucluse karst systems (Southeastern France). In: Crampon, N., Bakalowicz, M. (Eds.), Basic and Applied Hydrogeological Research in Frenh Karstic Areas, Montpellier Millau Workshop, European Commission, Brussels, pp. 27–35.

Noverraz, F., Bonnard, C., Dupraz, H., Huguenin, L., 1998. Grands glissements de versants et climat. Rapport final PNR 31, vdf hochschulverlag AG an der ETH Zürich, 314 p.

Olsson, O., Black, J., Gale, J., Holmes, D., 1998. Stripa Project-site characterization and validation-stage 4. Preliminary assesment and detail prediction. Stripa Project TR91-08, SKB, 1991, Stockholm, Sweden.

Pinder, G.F., Jones, J.F., 1969. Determination of the groundwater component of peak discharge from the chemistry of total runoff. Water Resour. Res. 15 (2), 438–445.

Pine, R.J., Cundall, P.A., 1985. Applications of the Fluid Rock Interaction Program (FRIP) to the Modeling of Hot Dry Geothermal Energy Systems, Proceedings of the International Symposium on Fundamentals of Rock Joints, Bjokiden, pp. 293–302.

Vengeon, J.M., Hantz, D., Giraud, A., Ract, D., 1996. Numerical modeling of rock slope deformations, International Symposium in Rock mechanics and Rock Engineering, Eurock '96, Ed. Barla, Torino, Italy, pp. 659–666.

Vengeon, J.M., 1998. Déformation et rupture des versants en terrain métamorphique anisotrope. PhD Thesis. University Joseph Fourier-Grenoble 1, 186 p.

Vinkler, F., 1999. Couplages hydromécaniques dans les massifs rocheux: du stockage de déchets radioactifs à la stabilité des mines abandonnées. PhD Thesis. Institut National Polytechnique de Lorraine, 200 p.

Witherspoon, P.A., Wang, J.S.Y., Iawi, K., Gale, J.E., 1980. Validity of cubic law for fluid flow in a deformable rock fracture. Water Resour. Res. 16 (6), 1016–1024.

Zhang, X., Sanderson, D.J., 1996. Effects of stress on the 2-D permeability tensor of natural fracture networks. J. Geophys. Int. 125, 912–924.